ISSN 2072-5981

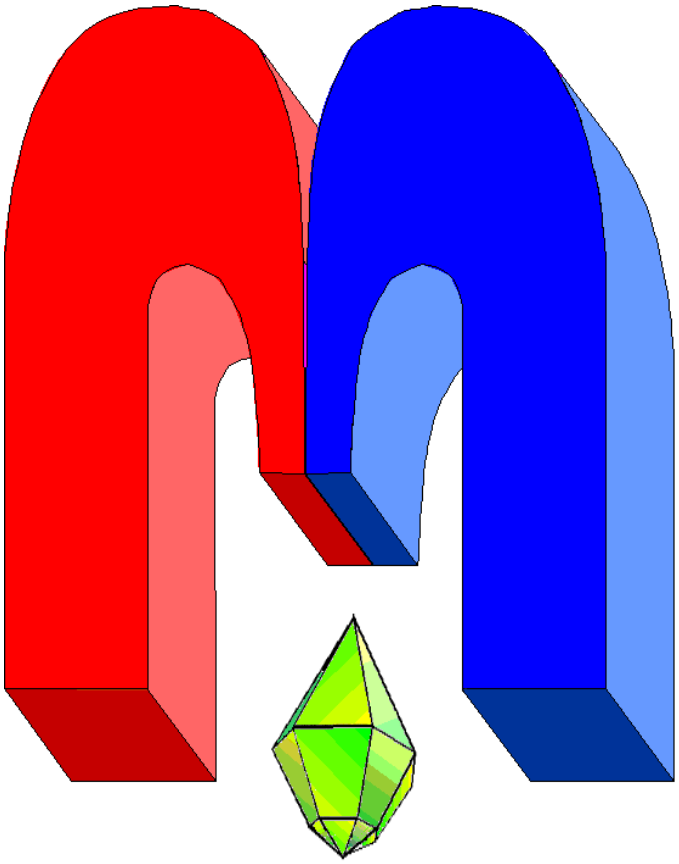

Magnetic Resonance in Solids

Electronic Journal

Volume **15**, **2013**
No. **1**, **13102** – 7 *pages*

http://mrsej.ksu.ru

Established and published by Kazan University
Sponsored by International Society of Magnetic Resonance (ISMAR)
Registered by Russian Federation Committee on Press, August 2, 1996
First Issue was appeared at July 25, 1997

"***Magnetic Resonance in Solids. Electronic Journal***" (**MRS*ej***) is a peer-reviewed, all electronic journal, publishing articles which meet the highest standards of scientific quality in the field of basic research of a magnetic resonance in solids and related phenomena. **MRS*ej*** is free for the authors (no page charges) as well as for the readers (no subscription fee). The language of **MRS*ej*** is English. All exchanges of information will take place via Internet. Articles are submitted in electronic form and the refereeing process uses electronic mail. All accepted articles are immediately published by being made publicly available by Internet ((http://**MRS*ej***.ksu.ru)).

---

* In Kazan University the Electron Paramagnetic Resonance (EPR) was discovered by Zavoisky E.K. in 1944.

Atherosclerotic plaque and hydroxyapatite nanostructures studied by high-frequency EPR†

M.R. Gafurov [1], B.V. Yavkin [1], T.B. Biktagirov [1], G.V. Mamin [1], S.B. Orlinskii [1, *], V.V. Izotov [1], M.Kh. Salakhov [1], E.S. Klimashina [2], V.I. Putlayev [2], V.A. Abdul'yanov [3], I.M. Ignatjev [3], R.N. Khairullin [3], A.V. Zamochkin [3], Yu.A. Chelyshev [1,4]

[1] Kazan Federal University, Institute of Physics, Kazan 420008, Russia

[2] M. V. Lomonosov Moscow State University, Department of Chemistry, Moscow 119992, Russia

[3] Interregional Clinic and Diagnostic Center, Kazan 420101, Russia

[4] Kazan State Medical University, 420012 Kazan, Russia

**E-mail: Sergei.Orlinskii@kpfu.ru*

(Received February 18, 2013; revised April 9, 2013; accepted April 13, 2013)

A series of nanosized (20 nm and larger) samples of hydroxyapatite powders synthesized by wet preparation method and doped with Mn^{2+} and Pb^{2+} ions were studied by 94 GHz pulsed electron paramagnetic resonance (EPR). The results are compared with those obtained in the samples of aorta walls from male patients with atherosclerosis as well as in bulk hydroxyapatite materials. It is shown that in contrast to bulk materials Pb ions at least partially replace the Ca(1) site in the hydroxyapatite structure. The spectral characteristics of the Mn^{2+} ions revealed in atherosclerotic plaque and synthetic hydroxyapatite are found to be practically identical. The hypothesis about the important role of (nano)hydroxyapatite in formation and rupture of atherosclerotic plaques is supported.

PACS: 83.80.Lz, 87.64.-t

Keywords: hydroxyapatite, nanomaterials, atherosclerotic plaque, EPR, ENDOR

1. Introduction

Initial interest to the study of the nanosized hydroxyapatite is governed by the search for reliable prognostic markers for atherosclerotic plaque development. *Plaque* (also known as *atheroma*) stands for fatty deposits within the coronary arteries in arteriosclerotic cardiovascular diseases (ASVD). ASVD is a condition in which an artery within the heart wall thickens and hardens. According to the current understanding, a large number of diseases with totally different clinical presentations are basically atherosclerosis related: myocardial infarction, stroke, abdominal aneurysms, lower limb ischemia, etc. The mortality rate in Russian Federation from the diseases of the blood circulatory system is reported to be about 800 on 100 000 (2009) [1-3].

Most of the acute manifestations of atherosclerosis share a common pathogenetic feature: rupture of an atherosclerotic plaque. Atherosclerotic plaque contains multiple components including lipidic, fibrotic, thrombotic, and calcific materials. The calcium deposits in cardiovascular tissues are comprised of various calcium salts, such as calcium carbonate, calcium oxalate, calcium phosphate, calcium pyrophosphate, and hydroxyapatite (HAp). It was proposed that exactly the microcalcification in thin fibrous caps is tightly connected with the instability of the plaque, leading to the plaque rupture [4]. X-ray diffraction (XRD), micro fluorescence (μXRF) analysis combined with the scanning microscopy (TEM) and electron paramagnetic resonance (EPR) measurements of postmortem samples of aorta walls from male patients with atherosclerosis at different stages show that the plaque growth and instability are tightly connected with the presence and size of the HAp component in the organomineralic matrix of aorta deposits [5]. It was proposed, therefore, that the nanosized HAp

† This paper is prepared on base of invited lecture at XV International Youth Scientific School "Actual problems of magnetic resonance and its application", Kazan, 22 – 26 October 2012 and it is published after additional MRSej reviewing.

components of the aorta tissues could serve at least as markers for the early diagnosis of the plaque rupture risks. Advantages of the increased resolution and sensitivity of high-frequency (94 GHz) EPR methods were demonstrated in paper [5] to detect and quantify early formation of HAp, i.e. the presence of the nanosized HAp in the aorta tissues at earlier ASVD stages. Microcalcification at advanced stage of the disease could be studied also by "routine" 9 GHz techniques.

The primary interest to the HAp-based nanomaterials is not restricted by only the atherosclerosis diagnosis. Hydroxyapatite is widely used as an implant to fill bone defects in orthopedics, maxillofacial surgery as well as in stomatology. It is thought that the nanosized HAp is the better candidate for an apatite substitute of bone in biomedical applications than micro-sized hydroxyapatite [6, 7]. HAp nanoparticles also have the potential to improve current disease diagnosis due to their ability to circulate in the blood to image tissues and cells or to deliver a payload for bio-imaging and therapeutical applications [8]. Antitumor effects of HAp nanoparticles are reported [9]. High sorption activity to a number of ions including those of some heavy metals and radio nuclides makes the HAp-based substances important not only for biomedical but also for waste management and in catalysts applications [8].

To realize the capabilities and limitations of modern EPR spectroscopy to study the nanosized HAp-based materials of organic and inorganic origin, we have investigated the plaque tissues and synthetic HAp nanoparticles by the high-frequency (94 GHz) EPR techniques.

2. Experimental

Plaque tissues of aorta walls from male patients with atherosclerosis at different stages were the same as investigated in paper [5]. The nanosized HAp-based materials with the average sizes of 20, 30 and 1000 nm were synthesized by the wet (precipitation) chemical procedure involving the aqueous solutions of calcium nitrate, diammonium hydrogen phosphate and ammonium hydroxide:

$$10\ Ca(NO_3)_2 + 6\ (NH_4)_2HPO_4 + 8NH_4OH \rightarrow Ca_{10}(PO_4)_6(OH)_2\downarrow + 20\ NH_4NO_3 + 6H_2O. \quad (1)$$

The main advantages of the process are: (a) high yield of targeted phase of HAp, (b) fast production rate, (c) low processing costs, (d) the only by-product consists of ammonium nitrate irreversibly decomposed at temperature higher than 210°C into two or three gases – water vapor and nitrogen (I) oxide, N_2O (below 270°C), or water vapor, nitrogen and oxygen (> 270°C). Its disadvantages are that it requires washing out of the precipitate to remove the nitrogen-containing residues and that the resulting product can be greatly affected by even a slight difference in the reaction conditions [10, 11].

Along with the "pure" HAp, the nanopowders of the HAps intentionally doped with manganese and lead ions were prepared by the same precipitation technique. Concerning Pb-containing HAp samples, 0.3 M stock solution of ammonium phosphate $(NH_4)_2HPO_4$ was added in a drop-wise manner under constant stirring in an atmosphere of gaseous N_2 (to avoid carbonate contamination) to 0.5 M stock solution containing calcium nitrate $Ca(NO_3)_2{\cdot}4H_2O$ and lead nitrate $Pb(NO_3)_2$ at desired ratio. The pH value of the stock solutions was pre-adjusted at 11.0 ± 0.5. The temperature was controlled and regulated at 80 ± 1°C. After total mixing of the stock solutions, the suspension was ripened and heated by use of a thermostatically controlled hot plate for 1 hour in one run (the case of 20 nm powder) and for 7 days in another run (1 μm powder) under constant stirring and N_2-bubbling. Then, the precipitates were filtered, thoroughly washed with 1 l of distilled water and allowed to dry at room temperature overnight. The Mn-containing samples were prepared in the same manner.

The powders were studied by FTIR spectroscopy in 400 - 4000 cm^{-1} range (to ensure the absence of carbonate and nitrogen containing species; Perkin-Elmer 1600, USA) and by XRD (Cu Kα radiation, Rigaku D/MAX 2500 with rotating anode, Japan). Sizes of crystallites were extracted from XRD line profile using Scherrer - and Wilson-formulas [12]. XRD analysis shows that all the samples

contain only one phase corresponding to the space group $P6_3/m$ with the parameters of the unit cell close to $a \approx b \approx 0.942$ nm and $c = 0.688$ nm typical for the bulk crystals of the hydroxyapatite. No significant difference in the positions of the XRD peaks was observed for the crystal sizes in the range of (20-1000 nm).

The micromorphology of the powders was examined by scanning and transmission electron microscopy (JEM-2000FX II, JEOL, Japan, operated at 200 kV; and FESEM LEO SUPRA 50VP, Carl Zeiss, Germany, 5 kV).

The Ca-, Pb- and P- contents of the powders were estimated by EDX XRF (INCA Energy+, Oxford Instruments, UK, attached to LEO SUPRA 50VP).

Pure HAp is EPR silent. X-ray irradiation of the synthesized Pb-containing nanopowders was performed using URS-55 tube ($U = 55$ kV, $I = 16$ mA, W-anticathode) at room temperature with the estimated dose of 10 kGy to create stable paramagnetic centres to have an ability to apply different EPR techniques. XRD patterns before and after X-ray irradiation were checked with Bruker D2 Phaser diffractometer and were the same.

Pulsed EPR and electron nuclear double resonance (ENDOR) measurements were done using high-frequency (94 GHz, W-band) Bruker Elexsys 680 spectrometer equipped with helium flow cryostats and different types of cavities. EPR spectra were recorded by means of field-swept two-pulse echo sequence $\pi/2 - \tau - \pi$ with the pulse length of the π pulse of (18 - 36) ns and time delay $\tau = 240$ ns. ENDOR spectra were detected utilizing the Mims sequence [13] with the duration of the radiofrequency pulse of 18 μs.

3. Results and Discussion

The electron spin echo (ESE) signal of atherosclerotic plaque and synthesized $Mn_{0.005}Ca_{9.995}(PO_4)_6(OH)_2$ (MnHAp) powder with the average grain size of 30 nm detected at room temperature during the magnetic field sweep (field-sweep ESE) in the W-band is shown in Fig. 1. The obtained six-line pattern signal (on top of other paramagnetic species presented in the plaque tissue) is stemmed from the hyperfine interaction between the electron ($S = 5/2$) and the nuclear ($I = 5/2$) spins of the incorporated manganese (Mn^{2+}) in non-oriented powders. Corresponding measurements of the transverse relaxation times of the manganese ions in the HAp samples and from the aorta derived species are presented in [14] wherein a possibility to use their values for the ASVD processes diagnostics is patented.

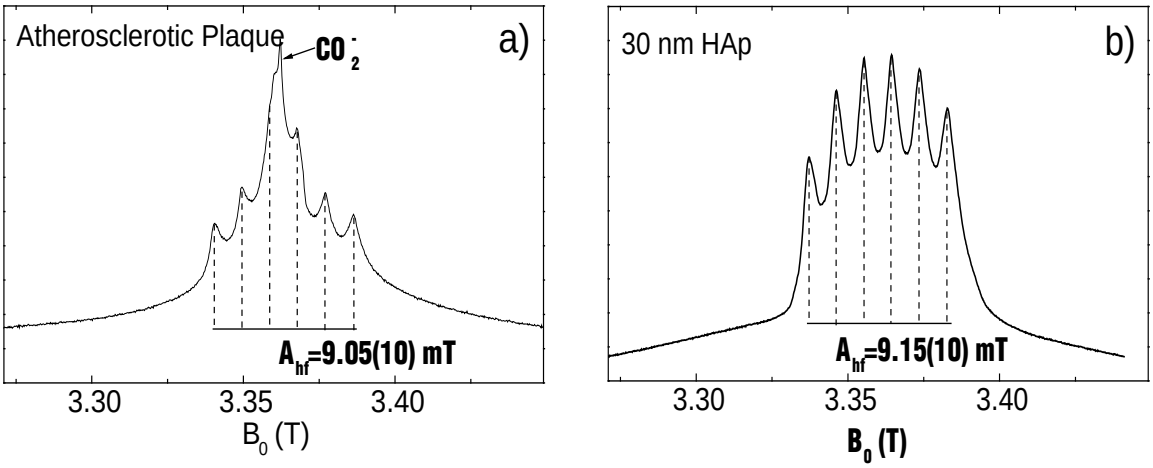

Figure 1. ESE-detected EPR spectra in the W-band of the atherosclerotic plaque (a) and of the nano-MnHAp (b) at $T = 293$ K.

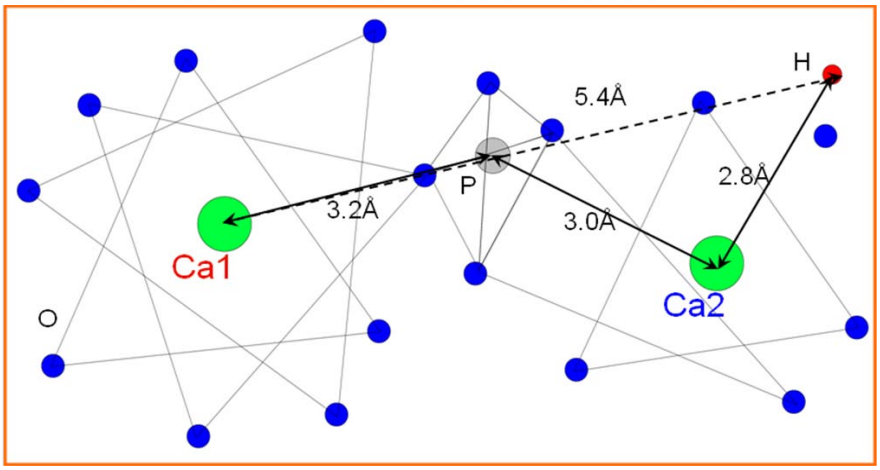

Figure 2. Schematic representation for two different Ca positions in hydroxyapatite crystal structure. The distances between Ca(1), Ca (2) and nearest P and H atoms are given [15].

Taking into account the accuracy of our experiments originating from the different sources of the magnetic field inhomogeneity at the sites of the studied paramagnetic centers, the identity of the observed spectroscopic parameters (*g*-factor and splitting constant of 9.1(1) mT) as well as the transverse relaxation times [14] point out that manganese in aorta samples is most probably located in HAp component of the plaque organomineralic matrix. This, in our opinion, is another piece of evidence that the nano-HAp structures play an important role in ASVD progression.

Two nonequivalent calcium positions Ca(1) and Ca(2) are present in the HAp structure [15]. The Ca(1) ions are arranged along a line parallel to the crystal *c*-axis and are connected to each other by three shared oxygen ions resulting in a “Ca(1) channel”. Ca(2) ion forms a triangle with two hydroxyl groups, and these triangles are perpendicular to the *c*-axis. This scheme is known as the “OH channel”. The 9-fold Ca(1) and 7-fold Ca(2) sites are both available for cationic substitution (Fig. 2). Knowledge of the substituent location could help one to understand the mechanisms of metal accumulation in body tissues and to differentiate the functions of the channels in biological processes.

Various studies have shown that small Mn^{2+} ions (ionic radius of 0.80 Å) prefer site Ca(1) in the case of calcium fluorapatite and becomes randomly distributed between the two sites in calcium chlorapatite [16]. The situation with the lead ions is much more controversial [17]. It is known that lead intoxication directly and indirectly alters many aspects of bone cell function [18]. High sorption activity of HAp based materials which are widely used in biomedical applications for Pb forced us to investigate the Pb-containing HAp nanopowders by EPR and ENDOR spectroscopy.

Synthesized HAp and $PbCa_9(PO_4)_6(OH)_2$ (Pb10HAp) species reveal no EPR response. It means that lead ions are incorporated into the HAp structure in the divalent state (Pb^{2+} ions are EPR silent due to the fully occupied 6*s* electronic shell). The EPR spectra of X-ray irradiated species are presented in Fig. 3. The EPR spectra are characterized by a pronounced hyperfine interaction (isotropic Fermi-contact-term) of the unpaired $6s^1$ electron with the nuclear moment $I = 1/2$ of the $^{207}Pb^{3+}$ isotope (natural abundance is 22.1%). It is manifested in the line splitting into two broad signals. The paramagnetic centres are characterized by $g = 1.982(2)$ and hyperfine constants of A(1 μm) = 24.74(5) GHz and A(20 nm) = 25.01(5) GHz.

Additional EPR lines detected in the magnetic fields of $B_0 < 2.65$ T and $B_0 > 3.85$ T disappear after annealing at 400°C and could be ascribed to $^{207}Pb^{3+}$ ions in the growth solution, i.e. to those paramagnetic centers that are not embedded into the HAp crystal lattice. Even isotopes of lead with the mass numbers of 204, 206 and 208 have no nuclear spin. Their EPR lines in the vicinity of $g \approx 2$ ($B_0 \approx 3.36$ T) overlap with the EPR spectra of other numerous radiation defects, are not shown in Fig. 3 and are not discussed in this work.

Superhyperfine interaction (characterized by the superhyperfine constant a) between the unpaired electron of Pb^{3+} ions in the $^2S_{1/2}$ ground state and neighbouring nuclei with $I = 1/2$ (here ^{31}P and ^1H) leads to the splitting of the ENDOR spectra (see Fig. 4) according to

$$\nu_{ENDOR} \propto h^{-1}|g^{(I)}\beta^{(I)}B_0 \pm a/2|, \quad (2)$$

where h is the Planck constant, $g^{(I)}$ is a nuclear g-factor and $\beta^{(I)}$ is a nuclear Bohr magneton [13].

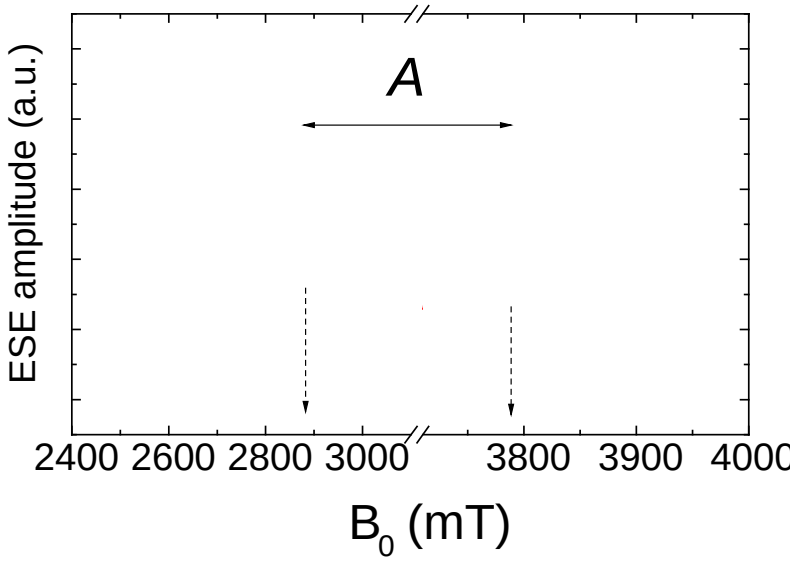

Figure 3. Echo-detected field-swept EPR spectrum of two irradiated Pb10HAP samples with the average nanocrystal sizes of 1 μm, (upper curve, red line) and of 20 nm (lower curve, black line) at $T = 20$ K. Vertical dashed arrows mark the B_0 values at which ENDOR spectra were taken.

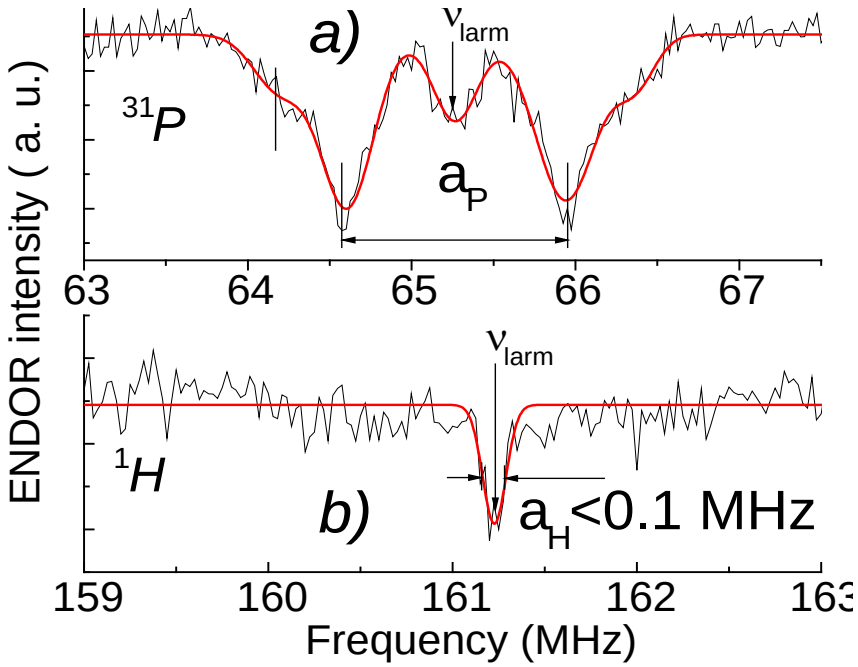

Figire 4. ENDOR spectra in the vicinity of Larmor frequencies of ^{31}P (a) with $a_P = 1.35(4)$ MHz and of ^1H (b) with $a_H < 0.1$ MHz measured in the magnetic field $B_0 = 3785$ mT at $T = 20$ K for the sample with the average crystal sizes of 20 nm. Noiseless red lines are the simulations in the dipole-dipole approximation with the parameters given in Table 1.

For the magnetic field positions corresponding to the maxima in the ESE spectra detected on the $^{207}Pb^{3+}$ ions (in the vicinity of B_0 = 2.9 T and 3.8 T, see Fig. 3) the values of a_P = 1.35(4) MHz and a_H < 0.1 MHz were extracted (Fig. 4), i.e. a significant difference between the a_P and a_H was observed.

Table 1. Parameters (d_H and d_P) used for the simulations of ENDOR spectra (Fig. 2). d_H is distance between the Pb^{3+} ion and hydrogen nuclei, and d_P is distance between the Pb^{3+} ion and phosphorous nuclei. Ca(1) and Ca(2) are the distances between the Ca and the nearest hydrogen and phosphorous atoms, correspondingly, according to the known literature data [15].

	Pb^{3+} ENDOR Simulation (nm)	Ca(1) (nm)	Ca(2) (nm)
d_H	0.53	0.54	0.28
d_P	0.34	0.32	0.30

Semiempirical and first-principle calculations performed for HAp in order to investigate the relative ion exchange ability with a number of divalent cations supported by the majority of XRD, XRF, FTIR and Raman spectroscopic experiments as well as by recent solid-state NMR measurements show an energetic preference for Pb^{2+} substitution at the Ca(2) site in bulk HAp materials (see [17] for the literature review). It correlates with the rule that the ions with the larger ionic radii and higher than Ca^{2+} electronegativity readily occupy Ca(2) positions.

Significant difference between the a_P and a_H observed in our experiments for $^{207}Pb^{3+}$ allows us to suggest that Pb^{3+} ions preferably replace Ca(1) position. The value of a, assuming the equal contribution from Fermi-contact overlapping of the wave functions of nuclei and ions in S - states, depends on the electron-nuclear dipole-dipole interaction, i.e. on electron-nucleus distance. Fig. 4 shows the simulation of the ENDOR spectra based on the calculation of the dipole-dipole interaction between the Pb^{3+} ions and nuclei involved averaged for the powder for all possible values of θ that is the angle between the direction of $\mathbf{B}_0$ and the main axis of the dipole with the distances given in Table 1. Good quantitative correspondence between the experimental and calculated data supports the statement that Pb^{3+} ions most probably occupy Ca(1) sites in HAp lattice (cf. Table 1, Fig. 2). It also means that Pb^{2+} ions (as precursors for the Pb^{3+} ions) at least partially occupy the Ca(1) positions in Pb10HAp species studied.

4. Summary

1. EPR of the manganese ions (Mn^{2+}) in the atherosclerotic plaques was detected. It is shown that the spectroscopic parameters of Mn^{2+} ions are practically the same for the investigated atherosclerotic plaques and synthesized HAp nanoparticels. This fact is a further proof of the hypothesis that hydroxyapatite plays an important role in formation/rupture of atherosclerotic plaques.

2. High sensitivity of modern commercially available high-frequency spectrometers opens new horizons for use of the EPR methods in biomedical research. In particular, for early ASVD diagnosis.

3. In the investigated Pb-containing nanosized HAp samples Pb^{3+} ions located in Ca(1) position in the hydroxyapatite structure are detected. Spectroscopic parameters of the $^{207}Pb^{3+}$ stable paramagnetic centers are measured with a high accuracy. Minor modifications of the hyperfine constant with the size of the nano-HAp powders are observed.

4. ENDOR results allow to admit that in the Pb-containing nano-Hap samples the Pb^{2+} ions as the precursors of Pb^{3+} are at least partially located at the Ca(1) site. It seems to be that the distribution of a dopant between Ca(1) and Ca(2) sites is defined not only by the radius and electronegativity of the dopant species but also is strongly affected by the preparation technique and conditions, size of the HAp nanocrystals, etc.

Acknowledgments

The work was supported by Russian Ministry of Science and Education (state contract No. 16.552.11.7083).

References

1. Petrukhin I.S., Lunina E.Y . *Public Health Reviews* **33**, 436 (2012)
2. Weissberg P.L. *Heart* **83**, 247 (2000)
3. *Global Atlas on cardiovascular disease prevention and control*, World Health Organization, Geneva, 155 p. (2011)
4. Vengrenyuk Y., Carlier S., Xanthos S., Cardoso L., Ganatos P., Virmani R., Einav Sh., Gilchrist L., Weinbaum S. *PNAS* **103**, 14678 (2006)
5. Abdul'yanov V.A., Galiullina L.F., Galyavich A.S., Izotov V.G., Mamin G.V., Orlinskii S.B., Rodionov A.A., Salakhov M.Kh., Silkin N.I., Sitdikova L.M., Khairullin R.N., Chelyshev Yu.A. *JETP Lett.* **88**, 69 (2008)
6. LeGeros R.Z, LeGeros J.P. Ch.16: Hydroxyapatite (pp. 367-394) in "*Bioceramics and their clinical applications*" by T. Kokubo (Ed.). Woodhead Pub. and Maney Pub., Cambridge, 760 p. (2008)
7. Dorozhkin S.V., Epple M. *Angew Chem Int Ed.* **41**, 3130 (2002)
8. Dorozhkin S.V. *Am. J. Biomed. Eng.* **2**, 48 (2012)
9. Chu S.H., Feng D.F., Ma Y.B., Li Z.Q. *Int J Nanomedicine* **7**, 3659 (2012)
10. Jarcho M., Bolen C.H., Thomas M.B., Bobick J., Kay J.F., Doremus R.H. *J. Mater. Sci.* **11**, 2027 (1976)
11. Kehoe Sh. Optimisation of Hydroxyapatite (HAp) for Orthopaedic Application via the Chemical Precipitation Technique *Ph.D. Thesis*, Dublin City University, 393 p (2008)
12. Keijser T.De, Langford J.I., Mittemeijer E.J., Vogels A.B.P. *J. Appl. Cryst.* **15**, 3087 (1982)
13. Murphy D.M., Farley R.D. *Chem. Soc. Rev.* **35**, 249 (2006)
14. Silkin N.I., Chelyshev Yu.A., Mamin G.V., Orlinskii S. B., Salakhov M. Kh. Patent RU 2468368
15. Elliott J.C. *Studies in Inorganic Chemistry* **18**, 1 (1994)
16. Nounah A., Maroufi N., Ichou Y., Ait Y, Lacout J.L., Savariault J.M. *J. Phys. IV* **123**, 251 (2005)
17. Yavkin B.V., Mamin G.V., Orlinskii S.B., Gafurov M.R., Salakhov M.Kh., Biktagirov T.B., Klimashina E.S., Putlayev V.I., Tretyakov Yu.D., Silkin N.I. *Phys. Chem. Chem. Phys.* **14**, 2246 (2012)
18. Pounds J.G., Long G.J., Rosen J.F. *Environ Health Perspect.* **91**, 17 (1991)